Materials Science and Engineering B 274 (2021) 115444

Contents lists available at ScienceDirect

Materials Science & Engineering B

journal homepage: www.elsevier.com/locate/mseb

Unvailing the spin–phonon coupling in nanocrystalline $BiFeO_3$ by resonant two-phonon Raman active modes

Bojan Stojadinović [a,*], Dejan M. Djokić [a], Novica Paunović [a], Ivica Živković [b], Luka Ćirić [c], Vladan Kusigerski [d], Zorana Dohčević-Mitrović [a,*]

[a] Institute of Physics Belgrade, University of Belgrade, Pregrevica 118, 11080 Belgrade, Serbia
[b] Laboratory for Quantum Magnetism, Institute of Physics, Ecole Polytechnique Féderale de Lausanne, CH-1015 Lausanne, Switzerland
[c] Laboratory of Nanostructures and Novel Electronic Materials, Ecole Polytechnique Féderale de Lausanne, CH-1015 Lausanne, Switzerland
[d] "Vinča" Institute of Nuclear Sciences, University of Belgrade, P.O. Box 522, Belgrade 11001, Serbia

ARTICLE INFO

Keywords:
$BiFeO_3$ nanomaterials
Sol–gel processes
Raman spectroscopy
Magnetic measurements
Spin–phonon interactions

ABSTRACT

We report on temperature dependence of two-phonon Raman spectra in $BiFeO_3$ nanocrystals, above and below the Néel temperature T_N using a resonant laser excitation line (λ = 532 nm). Two-phonon modes exhibited anomalous frequency hardening and deviation from the anharmonic decay below T_N. Such behavior strongly supported the existence of spin-two-phonon interaction, because these modes are known to be very sensitive to the antiferromagnetic ordering. Within the mean-field theory for the nearest-neighbor interaction, the linear relationship between spin–spin correlation function and observed two-phonon frequency shift below T_N was obtained. This approach enabled to quantify the spin–phonon interaction by spin–phonon coupling strength for both two-phonon modes and justified the application of mean-field approach. Magnetic measurements revealed the coexistence of antiferromagnetic and weak ferromagnetic phases below T_N, which were found non competitive, additionally supporting the mean-field approach from which we deduced that the two-phonon modes in $BiFeO_3$ are correlated with antiferromagnetic ordering below T_N.

1. Introduction

Multiferroic materials attract a lot of attention because of their multifunctional properties and interesting fundamental physics [1,2]. Among all the single-phase multiferroic materials studied so far, $BiFeO_3$ takes a prominent place because both ferroelectric (Curie temperature, $T_C \approx 1150$ K) and magnetic (Néel temperature, $T_N \approx 640$ K) transition temperatures are well above room temperature (RT). In bulk phase $BiFeO_3$ has G-type antiferromagnetic ordering (AFM), with a long period cycloidal modulation (62 nm) superimposed below T_N. Above T_N, $BiFeO_3$ becomes paramagnetic (PM) [3]. In nanophased $BiFeO_3$ spin spiral structure can be suppressed [4] and Dzyaloshinskii–Moriya (DM) interaction becomes important. DM interaction induces non-collinear spin states which compete with the exchange interaction that favors anti-parallel spin alignment providing a coexistence of ferromagnetic (FM) and antiferromagnetic ordering [2,5]. Furthermore, the appearance of strong magnetoelectric effect in epitaxial $BiFeO_3$ thin films [6] and nanoparticles [4], positions nanophased $BiFeO_3$ as a leading candidate material for spintronics, magnetic field sensor devices and ferroelectric non-volatile memories [1,5,7–9]. However, the coupling between magnetic and ferroelectric degrees of freedom in $BiFeO_3$ nanostructures still remains an open issue. Therefore, it is of great importance to study the interplay between lattice vibrations and magnetic excitations, because lattice distortion influences the ferroelectric polarization and accordingly affects its coupling to magnetic order. Furthermore, spin–phonon interaction is fundamental for driving relaxation in magnetic materials.

Among the optical spectroscopy methods, Raman spectroscopy proves to be a powerful experimental tool to elucidate spin–phonon (s-ph) interactions, since Raman mode can be sensitive to the spin correlations. In magnetic nanomaterials, such as $BiFeO_3$, optical phonon modes can be influenced by the exchange coupling between magnetic ions at and below the temperatures of magnetic phase transitions. The spin–phonon interaction usually manifests as atypical temperature dependence of Raman phonon frequency, linewidth or integrated intensity. From the deviation of the Raman mode frequency from the anharmonicity at and below the magnetic phase transition, it is possible to estimate the spin–phonon coupling strength in the antiferromagnets or ferromagnets. Being rather phenomenological, the approach developed by Lockwood and Cottam [10] treats the strength of the spin–phonon coupling through the emergence of the AFM order

* Corresponding authors.
E-mail addresses: bojans@ipb.ac.rs (B. Stojadinović), zordoh@ipb.ac.rs (Z. Dohčević-Mitrović).

https://doi.org/10.1016/j.mseb.2021.115444
Received 29 March 2021; Received in revised form 24 August 2021; Accepted 4 September 2021
Available online 25 September 2021

parameter, that is the sublattice magnetization, but not the net one. Moreover, it turns out that a thorough microscopic treatment due to Djokic et al. [11] further corroborates this fact whereby the majority of the AFM ordering contribution to the phonon spectra is observed through the magnitude of the sublattice magnetization. The influence of any weak FM ordering (canted or so) in the system upon spin–phonon strength is thus greatly overwhelmed by the AFM ordering. Phonon anomalies around and below T_N were observed in the first-order Raman spectra of $BiFeO_3$ single crystal [12,13], ceramics [14] and thin films [15,16] and were ascribed to the influence of spin correlations on the phonon energies. The pioneering works of Cazayous [17] and Ramirez [18] pointed at possible strong spin-two-phonon interaction in $BiFeO_3$ single crystals and thin films, but all above mentioned works were restricted to qualitative description of the effects of spin correlations on the Raman active first and second-order phonons without any deeper analysis of spin–phonon coupling mechanism.

In the light of these facts, to examine more thoroughly the coupling between lattice and spin degrees of freedom in nanocrystalline $BiFeO_3$, we investigated temperature-dependent second-order Raman spectra of $BiFeO_3$ nanocrystals in a wide temperature range below, at and above the Néel temperature using a resonant excitation line. The anomalous phonon hardening and obvious deviation from the anharmonicity of two-phonon Raman modes below Néel temperature was elaborated within a mean-field approach in order to correlate the spin–spin correlation function with observed frequency shift and to estimate the nearest-neighbor spin–phonon coupling constant. Magnetic measurements have shed more light on the nature of spin–phonon coupling mechanism in $BiFeO_3$ nanocrystals.

2. Experimental details

$BiFeO_3$ nanocrystals were synthesized by a sol–gel method and detailed sample preparation and characterization of the crystal structure and phase composition was given in Ref. [19]. $BiFeO_3$ nanoparticles were of spherical shape with average particle size of 64 nm deduced from SEM measurements [19,20]. Raman spectra of $BiFeO_3$ nanocrystals were collected in a backscattering geometry using TriVista 557 triple spectrometer with the spectral resolution of 2 cm^{-1}. Second-order Raman spectra of $BiFeO_3$ nanocrystals pressed into pellets were recorded between 80 and 723 K in the 1000–1500 cm^{-1} frequency range using a Linkam THMSG600 microscope heating stage. The resonant 532 nm line of a solid-state Nd:YAG laser was used as an excitation source, with output laser power low enough (less than 2 mW) to avoid the heating effects and/or sample thermal degradation. The Raman spectra were corrected by thermal occupation factor for the second-order scattering $S(\omega) = S_0(\omega)/(n+1)^2$, where $S_0(\omega)$ is measured intensity and $n = (e^{\hbar\omega/k_BT} - 1)^{-1}$ is the Bose–Einstein thermal occupation factor [21]. Magnetic measurements at and below 300 K were performed on a SQUID-based Quantum Design magnetometers MPMS-5T and MPMS XL-5.

3. Results and discussions

The room-temperature Raman spectrum of $BiFeO_3$ nanocrystalline sample in the range 40–1500 cm^{-1} is shown in Fig. 1.

Factor group analysis for the rhombohedral $R3c$ structure of $BiFeO_3$ predicts 13 Raman active modes ($4A_1 + 9E$), but the assignment of the Raman modes from the literature is somewhat controversial even in the case of $BiFeO_3$ single crystal Raman spectra measured or calculated in different polarizations [22–26]. As shown in Fig. 1, among the first order Γ-point phonons, modes around 79, 146, 175, 219, 261, 282, 332, 367, 435, 480 and 550 cm^{-1} are clearly seen. According to the polarized Raman spectra of $BiFeO_3$ single crystals [23,25], ceramics [27] and thin films [28] we assigned modes around 146, 175 and 219 cm^{-1} to A_1 modes and modes around 79, 261, 282, 332, 367, 435, 480 and 550 cm^{-1} to E modes. Beside these modes, weaker Raman modes at around 575 and 656 cm^{-1} and a stronger mode at ≈630 cm^{-1} are also observed. The 575 and 656 cm^{-1} modes (marked with * in Fig. 1) can be ascribed to the mullite-type ($Bi_2Fe_4O_9$) secondary phase [29], the presence of which has been confirmed from the X-ray diffraction analysis of $BiFeO_3$ nanocrystalline sample [19]. The Raman mode at ≈630 cm^{-1} is not a zone center mode [27,30]. According to Bielecki et al. [30] this mode can be assigned to the Raman inactive A_2 LO phonon mode which appears in $BiFeO_3$ thin films, ceramics and nanoparticles [18,30–33]. As can be seen in Fig. 1, the intense second-order Raman modes were observed above 1000 cm^{-1} and from now on we will focus our attention on the temperature behavior of these Raman modes.

The high-order Raman modes of the ferroelectric materials are usually very weak, but in the spectrum of $BiFeO_3$ from Fig. 1 an intense multiphonon band around 1000–1500 cm^{-1} is observed. This prominent band is already reported in $BiFeO_3$ thin films and single crystals [17,18,25], as well as in $BiFeO_3$ nanoparticles [31,32]. The broad band at 300 K from Fig. 1 was deconvoluted with Lorentzian type profile into four modes: mode at 1090 cm^{-1}, a strong mode at 1252 cm^{-1} and two low-intensity phonon modes at 1150 and 1330 cm^{-1}. The second-order modes at 1090 and 1252 cm^{-1}, labeled as S_1 and S_2 in Fig. 1, are, within the error limits, at the double frequency of the first-order Raman E mode at around 550 cm^{-1} and inactive A_2 mode at around 630 cm^{-1} [22,30]. These modes were ascribed to two-phonon modes in accordance with literature data [13,17,18,30], whereas the remaining two modes can be assigned to $2A_g$ modes of $Bi_2Fe_4O_9$ secondary phase [29]. Yang et al. [34] have investigated the behavior of two-phonon modes in $BiFeO_3$ powders using different excitation lines and reported that the intensity of two-phonon S_1 and S_2 modes are significantly enhanced under the 532 nm excitation. The intensity enhancement of S_1 and S_2 modes was attributed to the resonant enhancement when the excitation energy (532 nm ≈2.34 eV) is close to the absorption edge of $BiFeO_3$. The resonant behavior of these modes was explained by exchange mechanism between Fe^{3+} ions. Weber et al. [35] also reported resonant enhancement of second-order Raman modes in $BiFeO_3$ single crystals using 532 nm excitation, but suggested that in-gap electronic states like defect states from oxygen vacancies can be involved in the resonance process. Accordingly, we used 532 nm laser line in order to track the temperature evolution of S_1 and S_2 Raman modes. Two-phonon S_1 and S_2 modes are related to the Fe–O vibrations, i.e. octahedral rotations [17,18,32] which are very sensitive to the change of magnetic ordering. Moreover, it is well known that any perturbation of spiral spin structure in antiferromagnetic $BiFeO_3$ and distortion of FeO_6 octahedra due to the change of Fe–O–Fe bond angle can lead to the appearance of ferromagnetism [2,4,5]. Therefore, we have analyzed the behavior of S_1 and S_2 modes at temperatures below and above the magnetic phase transition.

In Fig. 2a are presented second-order Raman spectra in the 80–723 K temperature range. With increased temperature S_1 and S_2 modes gradually shift to lower wavenumbers and approaching the 600 K, the wavenumber shift is followed by a pronounced decrease of intensity (Fig. 2a). Similar behavior of S_2 mode was first observed by Ramirez [18] and Cazayous [17] and was ascribed to the coupling of S_2 mode with the magnetic sublattice. The accurate wavenumber change of S_1 and S_2 modes with temperature was obtained by deconvoluting the spectra from Fig. 2a with Lorentzian line shape function and Raman spectra at several representative temperatures together with cumulative fits are presented in Fig. 2b.

In magnetic materials, the change of phonon mode frequency with temperature can be expressed as [36,37]:

$$\omega(T) - \omega_0 \equiv \Delta\omega(T) = \Delta\omega_{lat}(T) + \Delta\omega_{anh}(T) + \Delta\omega_{e-ph}(T) + \Delta\omega_{s-ph}(T), \quad (1)$$

where $\omega(T)$ is measured frequency at temperature T and ω_0 is the harmonic mode frequency at $T = 0$ K. The first term on the right-hand side of the Eq. (1) is the frequency-independent pure-volume contribution due to the lattice expansion/contraction. The second term

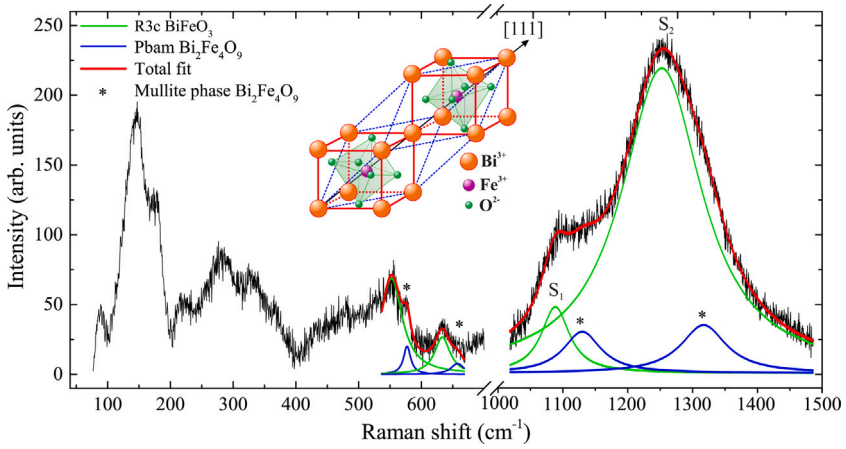

Fig. 1. Room-temperature Raman spectrum of nanocrystalline $BiFeO_3$ with Lorentzian fit (red line) of the first- and second-order phonon regions. The modes of mullite-type secondary phase $Bi_2Fe_4O_9$ are marked with (*). Inset represents the schematic of a pseudocubic unit cell including one formula unit with principle axis of polarization [111].

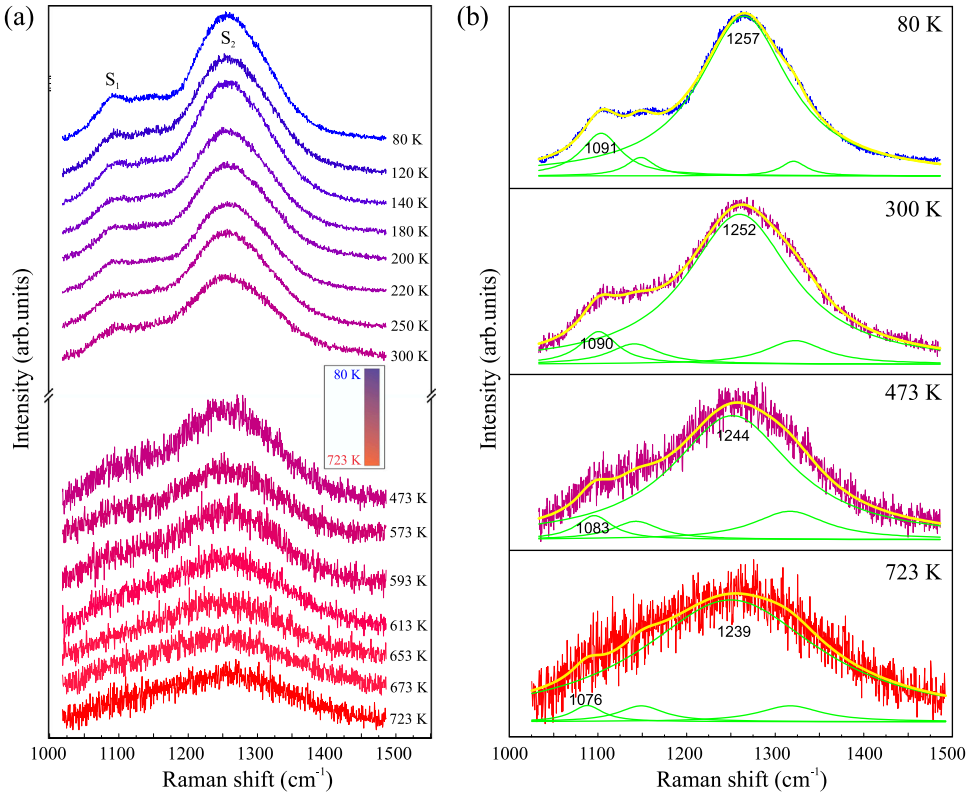

Fig. 2. Second-order Raman spectra of nanocrystalline $BiFeO_3$ (a) in the 80–723 K temperature range and (b) at selected temperatures. The solid lines represent Lorentzian fits of the experimental spectra.

is the anharmonic contribution due to phonon–phonon interactions. The last two terms account for the effects of renormalization of the phonon frequency due to electron–phonon and spin–phonon coupling.

In general, the change of phonon frequency due to pure-volume contribution is much smaller than the intrinsic anharmonic contribution, especially at low temperatures. $BiFeO_3$ in the form of powders or thin films is structurally stable up to 500 °C (773 K) [38] and any phonon frequency change due to lattice distortion is expected to be minimal, hence the first term can be neglected. The anharmonic interactions, significant at elevated temperatures, imply the phonon decay into two or three phonons, with a higher probability of the former. The phonon frequency change due to the decay of the phonon into two lower-energy phonons (three-phonon processes) can be expressed as [39,40]:

$$\Delta\omega_{\mathrm{anh}}(T) = A\left(1 + \frac{2}{e^{\frac{\hbar\omega(T)}{2k_B T}} - 1}\right), \tag{2}$$

where A is the anharmonic constant. In semiconductor materials like $BiFeO_3$, when the carrier concentration is low the third term can be ignored. Finally, the last term in Eq. (1) is the spin–phonon contribution, $\Delta\omega_{s-ph}(T)$, caused by the modulation of the exchange integral by lattice vibration [36]. In magnetic materials such as $BiFeO_3$, the phonon frequencies can be very sensitive to the spin correlations and in a case of Heisenberg model, Baltensberger and Helman [41] derived the relation for the shift of the phonon frequency due to the spin–phonon

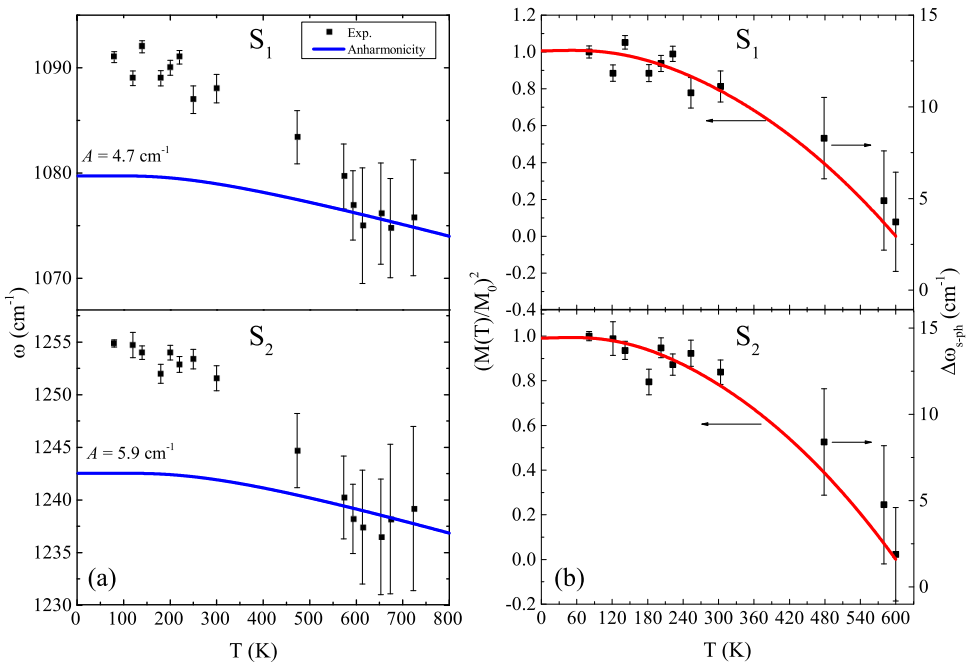

Fig. 3. (a) Temperature dependence of frequencies of the S_1 and S_2 two-phonon modes. The theoretically predicted anharmonic trend is presented by blue line together with the best fit anharmonic parameter (A). (b) Comparison of $(M(T)/M_0)^2$ (left) and $\Delta\omega_{s-ph}(T)$ (right) temperature dependences.

interaction,

$$\Delta\omega_{s-ph}(T) = -\lambda\langle S_i \cdot S_{i+1}\rangle, \quad (3)$$

where λ stands for the spin–phonon coupling constant and $\langle S_i \cdot S_{i+1}\rangle$ is the spin–spin correlation function between adjacent spins.

The temperature dependence of S_1 and S_2 mode frequencies (squares) is shown in Fig. 3a. As can be seen, at lower temperatures (T < 300 K) frequencies of S_1 and S_2 modes exhibit a slower change and at temperature around 600 K display step like anomaly. This temperature should coincide with Néel temperature, since there is no any known structural transition in $BiFeO_3$ at this temperature.

In order to determine the strength of spin–phonon coupling, it is necessary to separate spin–phonon and anharmonic contributions from the change of the phonon frequency with temperature. Knowing that phonon frequencies can be affected by AFM ordering below T_N and that the anharmonic processes should dominate over the spin–phonon coupling at high temperatures ($T > T_N$) for which the $BiFeO_3$ is in the PM state, the data for T > 593 K from Fig. 3a were fitted by Eq. (2) (blue line on Fig. 3a extrapolated to $T = 0$ K) in order to determine the anharmonic contribution to the phonon frequencies change. It is obvious that frequency change of both S_1 and S_2 modes below T_N show distinct deviation away from the expected anharmonic behavior. Similar frequency behavior has been observed in the Raman spectra of other antiferomagnetic [10,36,42–45] and ferromagnetic materials [46,47]. Thus, anomalous frequency hardening of S_1 and S_2 modes below T_N points out at the presence of spin-two-phonon coupling in nanocrystalline $BiFeO_3$. The difference between measured two-phonon frequencies from Fig. 3a and the calculated and extrapolated anharmonic behavior gives us the temperature dependent frequency shift due to spin–phonon interaction, $\Delta\omega_{s-ph}(T) = \omega(T) - \omega_{anh}(T)$. The $\Delta\omega_{s-ph}$ vs T dependence (squares) for S_1 and S_2 two-phonon modes is presented in Fig. 3b.

Within the mean-field approximation introduced by Weiss [48], spin–spin correlation function $\langle S_i \cdot S_{i+1}\rangle$ for adjacent spins at the ith and $(i+1)$th sites is proportional to the square of normalized magnetization, $(M(T)/M_0)^2$, and can be expressed as [49]

$$\frac{\langle S_i \cdot S_{i+1}\rangle}{S^2} = \left(\frac{M(T)}{M_0}\right)^2, \quad (4)$$

where $M(T)$ is in our case sublattice magnetization at temperature T and M_0 is the maximal value of sublattice magnetization. Having a look at Eqs. (3) and (4) it is obvious that $\Delta\omega_{s-ph}(T)$ should scale with $(M(T)/M_0)^2$ curve. The $(M(T)/M_0)^2$ curve was obtained using a numerical solution for Weiss equation in a case of Fe^{3+} ions having spin $S = 5/2$ [50] and then compared with experimentally obtained $\Delta\omega_{s-ph}(T)$ for both two-phonon modes, as presented in Fig. 3b. Obviously, for temperatures $T \leq T_N$, $\Delta\omega_{s-ph}(T)$ scales very good with $(M(T)/M_0)^2$ curve confirming that the significant deviation of S_1 and S_2 phonon frequencies from anharmonic behavior below T_N, i.e. the anomalous hardening, is actually due to spin–phonon interaction.

According to Eq. (3), from the plot $\Delta\omega_{s-ph}(T)$ vs $\langle S_i \cdot S_{i+1}\rangle(T)$ shown in Fig. 4 , the spin–phonon coupling constant λ can be determined for both two-phonon modes S_1 and S_2.

The red solid lines on Fig. 4 present the linear fit of the data from which the spin–phonon coupling constants λ_{S_1}=(2.54 ± 0.10) cm^{-1} and λ_{S_2}=(2.51 ± 0.10) cm^{-1} were determined. The linear behavior of $\Delta\omega_{s-ph}(T)$ vs $\langle S_i \cdot S_{i+1}\rangle(T)$ for the $T \leq T_N$ justifies the application of Eq. (3), implying that in the AFM phase spin–phonon coupling dominates over the anharmonicity and terminates in the paramagnetic phase. Furthermore, the fact that both two-phonon modes exhibit anomalous frequency hardening below magnetic ordering temperature and that the values for λ are very similar, indicates that there is a universal influence of the AFM magnetic ordering upon the two-phonon spectra.

Up to now it is well established that in antiferromagnetic $BiFeO_3$ nanoparticles with particle size close to or less than the period of spin cycloid appear ferromagnetic phase at room temperature [4,51–53]. $BiFeO_3$ nanoparticles can be considered to be composed of AFM core and FM shell giving rise to changes in the magnetic characteristics [53] or to the appearance of exchange bias and training effects [[52], and references within]. Since our $BiFeO_3$ nanoparticles are of the average size close to the spin cycloid period, we performed magnetic measurements in order to get better insight into the two-phonon Raman modes coupling with magnetic ordering below T_N.

Fig. 5a presents room-temperature magnetization (M) vs magnetic field (H) dependence for $BiFeO_3$ nanoparticles. From the M–H loop it can be seen that the magnetization curve (black circles) displays

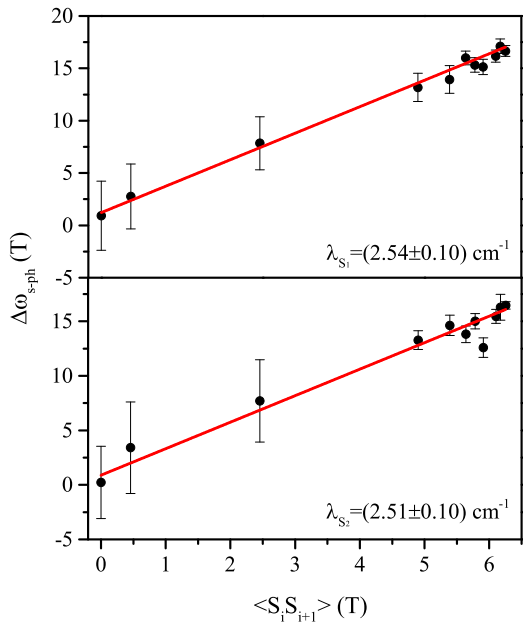

Fig. 4. The plot $\Delta\omega_{s-ph}(T)$ vs $\langle S_i \cdot S_{i+1}\rangle(T)$ for both two-phonon modes S_1 and S_2. The λ values for both modes were determined from the linear fit (red solid line) of the data. (For interpretation of the references to color in this figure legend, the reader is referred to the web version of this article.)

a hysteresis in the low-field region, indicating a presence of weak ferromagnetism. The FM component is superimposed over a linear background from antiferromagnetic $BiFeO_3$ phase and paramagnetic mullite phase. After subtracting the linear background, the ferromagnetic hysteresis curve (red squares) with the saturation magnetization value $M_S = 0.094$ emu/g was obtained. The inset in Fig. 5a displays the magnification of the hysteresis loop in the low-field region. The FM ordering can be considered as genuine one and does not originate from mullite or iron oxide impurity phases. Namely, mullite ($Bi_2Fe_4O_9$) phase is paramagnetic at room temperature and undergoes a transition to an antiferromagnetic state at $T_N \approx 264$ K [54]. Besides, the presence of iron oxides, leads to significantly enhanced ferromagnetism with large values of saturation magnetization [55]. The origin of FM ordering in otherwise antiferromagnetic $BiFeO_3$ is usually ascribed to the suppression of the spiral spin structure in particles with diameter less than the period of spin cycloid (62 nm) and higher distortion of FeO_6 octahedra or to the uncompensated spins on the nanoparticle surface. All of these effects lead to enhanced Dzyaloshinskii–Moriya interaction and appearance of ferromagnetism in nanocrystalline $BiFeO_3$ [2,4,52,56]. In that case $BiFeO_3$ nanoparticles can be considered to be constituted of core/shell structure, i.e. antiferromagnetic core and ferromagnetic shell. As our nanocrystalline $BiFeO_3$ powders are composed of nanoparticles with average particle size of 64 nm [19,20] it can be supposed that the interruption of long-range AFM ordering takes place primarily on the nanoparticle surface. This assumption is supported by a report of Huang et al. [4] who have shown that $BiFeO_3$ nanoparticles of core–shell structure, with size close to the period of spin cycloid, exhibit increased ferromagnetism. It was further argued that FM ordering originates not only from the surface uncompensated spins, but from enhanced distortion of FeO_6 octahedra around the [111] direction. Such enhanced structural distortion can cause suppression of spiral spin structure and strengthening of DM interaction responsible for the appearance of FM. Accordingly, both effects, the suppression of spin cycloid and uncompensated surface spins, can lead to the occurrence of weak ferromagnetism in our sample.

Fig. 5b displays zero field cooled (ZFC) and field cooled (FC) magnetization curves, measured at 1000 Oe. The ZFC and FC curves started to split below 250 K and the divergence became more pronounced with decreasing temperature. The ZFC curve showed a peak around the temperature of spin reorientation transition (200 K) [17,57] at which the Fe^{3+} magnetic moments are canted out of cycloidal plane. Besides, ZFC curve does not tend to $M = 0$ with approaching $T = 0$, as one would expect in a case of the presence of iron oxide impurity phases [58]. The ZFC/FC magnetization curves of our sample are very different from the ZFC/FC magnetization behavior of $BiFeO_3$ single crystal which was ascribed to the spin-glass ordering [59]. Recent ZFC/FC measurements on $BiFeO_3$ nanoparticles with sizes close to or less than the period of spin cycloid [4,7,56] have shown similar pronounced splitting of the ZFC/FC curves when antiferromagnetic and ferromagnetic orderings co-exist. Unlike the $BiFeO_3$ single crystal with antiferromagnetic ordering, those $BiFeO_3$ nanostructures can be considered as core–shell structures composed of antiferromagnetic core and ferromagnetic shell [4,52,56] in which more pronounced ZFC/FC splitting than in bulk $BiFeO_3$ suggests some irreversible effect on magnetic properties like breaking of AFM order and appearance of ferromagnetism [4,7,51,52]. Furthermore, more detailed analysis of ZFC/FC magnetization measurements on nanocrystalline $BiFeO_3$ [53] has shown that pronounced ZFC/FC splitting more likely originates from the changes in the domain structure at low temperatures and eventual antiferromagnetic domain pinning effect [4] than from spin-glass ordering.

In order to justify the use of mean-field theory approximation which does not include magnetic frustrations nor quantum fluctuations apart from the temperature ones [49], we refer to the study of Rao et al. on polycrystalline $BiFeO_3$ [60], where one can infer from that the Curie–Weiss temperature (θ_{CW}) tends to a very large value. Knowing that in bulk $BiFeO_3$ $T_N = 640$ K [1,2] and in nanostructured $BiFeO_3$ T_N slightly decreases with decreasing crystallite size [61], the $BiFeO_3$ is only seemingly frustrated system, since the frustration factor, $f = |\theta_{CW}|/T_N$ can exceed low frustration values [62]. However, we find magnetic frustration inconsequential because of the two noncompeting magnetic interactions: antiferromagnetic and ferromagnetic. These interactions are known to be cooperative in forming the stable Néel phase like in $MnSe_2$ [11]. Therefore, even at low temperatures, the average value of the relevant spin component per site is nearly 5/2, implying the stability of the AFM phase in $BiFeO_3$. Otherwise, spin–phonon coupling would be more complex, the $\Delta\omega_{s-ph}(T)$ would substantially deviate from the mean-field approximation model which we applied [44,47] and a different treatment of the spin–phonon coupling mechanism would be required. The presented magnetic measurements are in favor of the picture in which nothing else, but the AFM magnetic ordering, without the presence of magnetic frustrations, influences the anomalous hardening of two-phonon Raman modes below T_N in nanocrystalline $BiFeO_3$.

4. Concluding remarks

In conclusion, we have investigated the temperature evolution of the resonant Raman two-phonon modes in $BiFeO_3$ nanocrystals, which are known to be very sensitive to magnetic ordering. Temperature studies have shown anomalous hardening and significant deviation of two-phonon frequencies from the anharmonicity below Néel temperature. The anomalous phonon hardening was ascribed to spin-two-phonon coupling. Within the mean-field approach, the spin–spin correlation function was correlated to the two-phonon frequency shift and the spin–phonon coupling strength for two-phonon modes was derived. The linear relation between spin–spin correlation function and frequency shift below Néel temperature confirmed no presence of fluctuations or magnetic frustrations and justified the application of mean-field approach. Magnetic measurements revealed the presence of weak FM phase below T_N. The coexistence of AFM and FM ordering were found not competitive, justifying the conclusion derived from mean-field approach that two-phonon Raman modes below T_N are strongly coupled to AFM ordering.

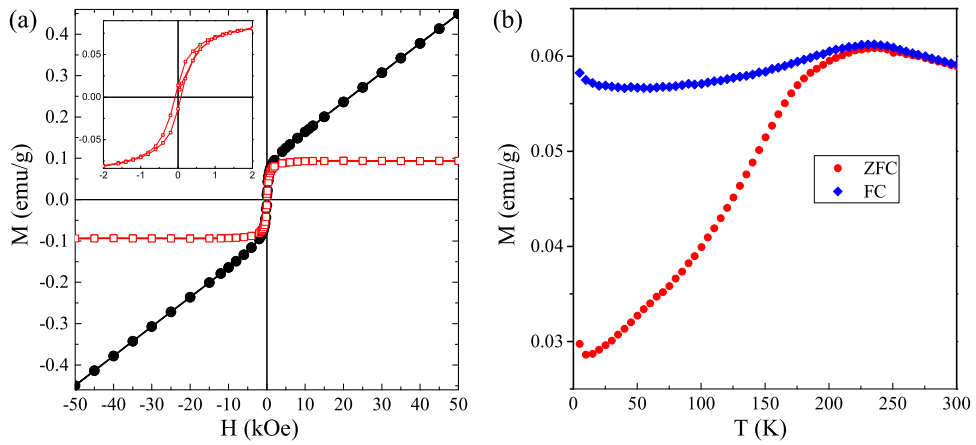

Fig. 5. (a) Room-temperature magnetization (M) vs magnetic field (H) dependence for $BiFeO_3$ nanoparticles, before (circles) and after subtraction (squares) of the linear background component. Inset shows zoom in view of M–H curve. (b) ZFC and FC magnetization curves measured at $H = 1000$ Oe.

Declaration of competing interest

The authors declare that they have no known competing financial interests or personal relationships that could have appeared to influence the work reported in this paper.

Acknowledgments

The authors greatly acknowledge funding provided by the Institute of Physics Belgrade, through the grant by the Ministry of Education, Science, and Technological Development of the Republic of Serbia.

References

[1] N.A. Spaldin, Multiferroics: Past, present, and future, Phys. Today 63 (2010) 38–43, http://dx.doi.org/10.1063/1.3502547.

[2] G. Catalan, J.F. Scott, Physics and applications of Bismuth ferrite, Adv. Mater. 21 (2009) 2463–2485, http://dx.doi.org/10.1002/adma.200802849.

[3] I. Sosnowska, T.P. Neumaier, E. Steichele, Spiral magnetic ordering in bismuth ferrite, J. Phys. C: Solid State 15 (1982) 4835–4846, http://dx.doi.org/10.1088/0022-3719/15/23/020.

[4] F. Huang, Z. Wang, J. Zhang, K. Min, W. Lin, R. Ti, T. Xu, J. He, C. Yue, J. Zhu, Peculiar magnetism of $BiFeO_3$ nanoparticles with size approaching the period of the spiral spin structure, Sci. Rep. 3 (2013) 2907–2913, http://dx.doi.org/10.1038/srep02907.

[5] C.-H. Yang, D. Kan, I. Takeuchi, V. Nagarajan, J. Seidel, Doping $BiFeO_3$: approaches and enhanced functionality, Phys. Chem. Chem. Phys. 14 (2012) 15953–15962, http://dx.doi.org/10.1039/C2CP43082G.

[6] J. Wang, J.B. Neaton, H. Zheng, V. Nagarajan, S.B. Ogale, B. Liu, D. Viehland, V. Vaithyanathan, D.G. Schlom, U.V. Waghmare, N.A. Spaldin, K.M. Rabe, M. Wuttig, R. Ramesh, Epitaxial $BiFeO_3$ multiferroic thin film heterostructures, Science 299 (2003) 1719–1722, http://dx.doi.org/10.1126/science.1080615.

[7] J. Wu, S. Mao, Z.-G. Ye, Z. Xie, L. Zheng, Room-temperature ferromagnetic/ferroelectric $BiFeO_3$ synthesized by a self-catalyzed fast reaction process, J. Mater. Chem. 20 (2010) 6512–6516, http://dx.doi.org/10.1039/c0jm00729c.

[8] J. Ma, J. Hu, Z. Li, C.-W. Nan, Recent progress in multiferroic magnetoelectric composites: from bulk to thin films, Adv. Mater. 23 (2011) 1062–1087, http://dx.doi.org/10.1002/adma.201003636.

[9] R. Ramesh, N.A. Spaldin, Multiferroics: progress and prospects in thin films, Nature Mater. 6 (2007) 21–29, http://dx.doi.org/10.1038/nmat1805.

[10] D.J. Lockwood, M.G. Cottam, The spin-phonon interaction in FeF_2 and MnF_2 studied by Raman spectroscopy, J. Appl. Phys. 64 (1988) 5876–5878, http://dx.doi.org/10.1063/1.342186.

[11] D.M. Djokić, Z.V. Popović, F.R. Vukajlović, Influence of antiferromagnetic spin ordering on the far-infrared active optical phonon modes of αMnSe, Phys. Rev. B 77 (2008) 014305, http://dx.doi.org/10.1103/PhysRevB.77.014305.

[12] C.-S. Chen, C.-S. Tu, P.-Y. Chen, V.H. Schmidt, Z.-R. Xu, Y. Ting, Spin-lattice coupling phase transition and phonon anomalies in bismuth ferrite $BiFeO_3$, J. Alloy. Compd. 687 (2016) 442–450, http://dx.doi.org/10.1016/j.jallcom.2016.06.193.

[13] T.M.H. Nguyen, X.N. Nguyen, X.-B. Chen, X.T. To, S. Lee, T.H. Nguyen, I.-S. Yang, Study of spin-phonon coupling in multiferroic $BiFeO_3$ through Raman spectroscopy, J. Mol. Struct. 1222 (2020) 128884, http://dx.doi.org/10.1016/j.molstruc.2020.128884.

[14] J. Wei, C. Wu, Y. Liu, Y. Guo, T. Yang, D. Wang, Z. Xu, R. Haumont, Structural distortion, spin-phonon coupling, interband electronic transition, and enhanced magnetization in rare-earth-substituted bismuth ferrite, Inorg. Chem. 56 (2017) 8964–8974, http://dx.doi.org/10.1021/acs.inorgchem.7b00914.

[15] M.K. Singh, W. Prellier, H.M. Jang, R.S. Katiyar, Anomalous magnetic ordering induced spin-phonon coupling in $BiFeO_3$ thin films, Solid State Commun. 149 (2009) 1971–1973, http://dx.doi.org/10.1016/j.ssc.2009.07.036.

[16] A. Ahlawat, S. Satapathy, S. Maan, V.G. Sathe, P.K. Gupta, Correlation of structure and spin-phonon coupling in (La, Nd) doped $BiFeO_3$ films, J. Raman Spectrosc. 45 (2014) 958–962, http://dx.doi.org/10.1002/jrs.4573.

[17] M. Cazayous, A. Sacuto, D. Lebeugle, D. Colson, Possible interplay between a two phonon mode and high energy magnetic excitations in $BiFeO_3$, Eur. Phys. J. B 67 (2009) 209–212, http://dx.doi.org/10.1140/epjb/e2009-00033-7.

[18] M.O. Ramirez, M. Krishnamurthi, S. Denev, A. Kumar, S.-Y. Yang, Y.-H. Chu, E. Saiz, J. Seidel, A.P. Pyatakov, A. Bush, D. Viehland, J. Orenstein, R. Ramesh, V. Gopalan, Two-phonon coupling to the antiferromagnetic phase transition in multiferroic $BiFeO_3$, Appl. Phys. Lett. 92 (2008) 022511, http://dx.doi.org/10.1063/1.2829681.

[19] B. Stojadinović, Z. Dohčević-Mitrović, D. Stepanenko, M. Rosić, I. Petronijević, N. Tasić, N. Ilić, B. Matović, B. Stojanović, Dielectric and ferroelectric properties of Ho-doped $BiFeO_3$ nanopowders across the structural phase transition, Ceram. Int. 43 (2017) 16531–16538, http://dx.doi.org/10.1016/j.ceramint.2017.09.038.

[20] D.M. Djokić, B. Stojadinović, D. Stepanenko, Z. Dohčević-Mitrović, Probing charge carrier transport regimes in $BiFeO_3$ nanoparticles by Raman spectroscopy, Scr. Mater. 181 (2020) 6–9, http://dx.doi.org/10.1016/j.scriptamat.2020.02.008.

[21] S.S. Mitra, Infrared and Raman spectra due to lattice vibrations, Springer US, Boston, MA, 1969, pp. 398–400, http://dx.doi.org/10.1007/978-1-4757-1123-3-14.

[22] R. Palai, R.S. Katiyar, H. Schmid, P. Tissot, S.J. Clark, J. Robertson, S.A.T. Redfern, G. Catalan, J.F. Scott, β Phase and γ-β metal-insulator transition in multiferroic $BiFeO_3$, Phys. Rev. B 77 (2008) 014110, http://dx.doi.org/10.1103/PhysRevB.77.014110.

[23] M. Cazayous, D. Malka, D. Lebeugle, D. Colson, Electric field effect on $BiFeO_3$ single crystal investigated by Raman spectroscopy, Appl. Phys. Lett. 91 (2007) 071910, http://dx.doi.org/10.1063/1.2771380.

[24] C. Beekman, A.A. Reijnders, Y.S. Oh, S.W. Cheong, K.S. Burch, Raman study of the phonon symmetries in $BiFeO_3$ single crystals, Phys. Rev. B 86 (2012) 020403, http://dx.doi.org/10.1103/PhysRevB.86.020403.

[25] H. Fukumura, S. Matsui, H. Harima, T. Takahashi, T. Itoh, K. Kisoda, M. Tamada, Y. Noguchi, M. Miyayama, Observation of phonons in multiferroic $BiFeO_3$ single crystals by Raman scattering, J. Phys. Condens. Mat. 19 (2007) 365224, http://dx.doi.org/10.1088/0953-8984/19/36/365224.

[26] P. Hermet, M. Goffinet, J. Kreisel, P. Ghosez, Raman and infrared spectra of multiferroic bismuth ferrite from first principles, Phys. Rev. B 75 (2007) 220102, http://dx.doi.org/10.1103/PhysRevB.75.220102.

[27] J. Hlinka, J. Pokorny, S. Karimi, I.M. Reaney, Angular dispersion of oblique phonon modes in $BiFeO_3$ from micro-Raman scattering, Phys. Rev. B 83 (2011) 020101, http://dx.doi.org/10.1103/PhysRevB.83.020101.

[28] M.K. Singh, H.M. Jang, S. Ryu, M.-H. Jo, Polarized Raman scattering of multiferroic $BiFeO_3$ epitaxial films with rhombohedral $R3c$ symmetry, Appl. Phys. Lett. 88 (2006) 042907, http://dx.doi.org/10.1063/1.2168038.

[29] M.N. Iliev, A.P. Litvinchuk, V.G. Hadjiev, M.M. Gospodinov, V. Skumryev, E. Ressouche, Phonon and magnon scattering of antiferromagnetic $Bi_2Fe_4O_9$, Phys. Rev. B 81 (2010) 024302, http://dx.doi.org/10.1103/PhysRevB.81.024302.

[30] J. Bielecki, P. Svedlindh, D.T. Tibebu, S. Cai, S.-G. Eriksson, L. Börjesson, C.S. Knee, Structural and magnetic properties of isovalently substituted multiferroic $BiFeO_3$: Insights from Raman spectroscopy, Phys. Rev. B 86 (2012) 184422, http://dx.doi.org/10.1103/PhysRevB.86.184422.

[31] S. Chauhan, M. Kumar, P. Pal, Substitution driven structural and magnetic properties and evidence of spin phonon coupling in Sr-doped $BiFeO_3$ nanoparticles, RSC Adv. 6 (2016) 68028–68040, http://dx.doi.org/10.1039/C6RA11021E.

[32] M. Kumar, M. Arora, S. Chauhan, S. Joshi, Raman spectroscopy probed spin-two phonon coupling and improved magnetic and optical properties in Dy and Zr substituted $BiFeO_3$ nanoparticles, J. Alloy. Compd. 692 (2017) 236–242, http://dx.doi.org/10.1016/j.jallcom.2016.09.031.

[33] B. Stojadinović, Z. Dohčević-Mitrović, N. Paunović, N. Ilić, N. Tasić, I. Petronijević, D. Popović, B. Stojanović, Comparative study of structural and electrical properties of Pr and Ce doped $BiFeO_3$ ceramics synthesized by auto-combustion method, J. Alloy. Compd. 657 (2016) 866–872, http://dx.doi.org/10.1016/j.jallcom.2015.09.235.

[34] Y. Yang, J.Y. Sun, K. Zhu, Y.L. Liu, J. Chen, X.R. Xing, Raman study of $BiFeO_3$ with different excitation wavelengths, Physica B 404 (2009) 171–174, http://dx.doi.org/10.1016/j.physb.2008.10.029.

[35] M.C. Weber, M. Guennou, C. Toulouse, M. Cazayous, Y. Gillet, X. Gonze, J. Kreisel, Temperature evolution of the band gap in $BiFeO_3$ traced by resonant Raman scattering, Phys. Rev. B 93 (2016) 125204, http://dx.doi.org/10.1103/PhysRevB.93.125204.

[36] E. Granado, A. Garcí a, J.A. Sanjurjo, C. Rettori, I. Torriani, F. Prado, R.D. Sánchez, A. Caneiro, S.B. Oseroff, Magnetic ordering effects in the Raman spectra of $La_1 - xMn_1 - xO_3$, Phys. Rev. B 60 (1999) 11879–11882, http://dx.doi.org/10.1103/PhysRevB.60.11879.

[37] X.-B. Chen, N.T. Minh Hien, K. Han, J. Chul Sur, N.H. Sung, B.K. Cho, I.-S. Yang, Raman studies of spin-phonon coupling in hexagonal $BaFe_{12}O_{19}$, J. Appl. Phys. 114 (2013) 013912, http://dx.doi.org/10.1063/1.4812575.

[38] J. Ryu, C.-W. Baek, D.-S. Park, D.-Y. Jeong, Multiferroic $BiFeO_3$ thick film fabrication by aerosol deposition, Met. Mater. Int. 16 (2010) 639–642, http://dx.doi.org/10.1007/s12540-010-0818-9.

[39] P.G. Klemens, Anharmonic decay of optical phonons, Phys. Rev. 148 (1966) 845–848, http://dx.doi.org/10.1103/PhysRev.148.845.

[40] M. Balkanski, R.F. Wallis, E. Haro, Anharmonic effects in light scattering due to optical phonons in silicon, Phys. Rev. B 28 (1983) 1928–1934, http://dx.doi.org/10.1103/PhysRevB.28.1928.

[41] W. Baltensperger, J.S. Helman, Influence of magnetic order in insulators on the optical phonon frequency, Helv. Phys. Acta 41 (1968) 668–673, http://dx.doi.org/10.5169/seals-113910.

[42] E. Aytan, B. Debnath, F. Kargar, Y. Barlas, M.M. Lacerda, J. Li, R. Lake, J. Shi, A.A. Balandin, Spin-phonon coupling in antiferromagnetic nickel oxide, Appl. Phys. Lett. 111 (2017) 252402, http://dx.doi.org/10.1063/1.5009598.

[43] P.-H. Shih, C.-L. Cheng, S.Y. Wu, Short-range spin-phonon coupling in in-plane CuO nanowires: a low-temperature Raman investigation, Nanoscale Res. Lett. 8 (2013) 1–6, http://dx.doi.org/10.1186/1556-276X-8-398.

[44] C. Kant, J. Deisenhofer, T. Rudolf, F. Mayr, F. Schrettle, A. Loidl, V. Gnezdilov, D. Wulferding, P. Lemmens, V. Tsurkan, Optical phonons, spin correlations, and spin-phonon coupling in the frustrated pyrochlore magnets $CdCr_2O_4$ and $ZnCr_2O_4$, Phys. Rev. B 80 (2009) 214417–214426, http://dx.doi.org/10.1103/PhysRevB.80.214417.

[45] J. Zhang, Q. Lian, Z. Pan, W. Bai, J. Yang, Y. Zhang, X. Tang, J. Chu, Spin-phonon coupling and two-magnons scattering behaviors in hexagonal NiAs-type antiferromagnetic MnTe epitaxial films, J. Raman Spectrosc. 51 (2020) 1383–1389, http://dx.doi.org/10.1002/jrs.5928.

[46] M.N. Iliev, M.V. Abrashev, A.P. Litvinchuk, V.G. Hadjiev, H. Guo, A. Gupta, Raman spectroscopy of ordered double perovskite La_2CoMnO_6 thin films, Phys. Rev. B 75 (2007) 104118, http://dx.doi.org/10.1103/PhysRevB.75.104118.

[47] R.X. Silva, M.C.C. Júnior, S. Yáñez-Vilar, M.S. Andújar, J. Mira, M.A. Señarís-Rodríguez, C.W.A. Paschoal, Spin-phonon coupling in multiferroic Y_2CoMnO_6, J. Alloy. Compd. 690 (2017) 909–915, http://dx.doi.org/10.1016/j.jallcom.2016.07.010.

[48] B.D. Cullity, C.D. Graham, Introduction to magnetic materials, Second Edition, Wiley-IEEE Press, New Jersey, 2008, pp. 91–99, http://dx.doi.org/10.1002/9780470386323.

[49] K. Yosida, Theory of magnetism, Springer-Verlag Berlin Heidelberg, 1996, pp. 72–74.

[50] V. Barsan, V. Kuncser, Exact and approximate analytical solutions of Weiss equation of ferromagnetism and their experimental relevance, Phil. Mag. Lett. 97 (2017) 359–371, http://dx.doi.org/10.1080/09500839.2017.1366081.

[51] K.P. Remya, D. Prabhu, R.J. Joseyphus, A.C. Bose, C. Viswanathan, N. Ponpandian, Tailoring the morphology and size of perovskite $BiFeO_3$ nanostructures for enhanced magnetic and electrical properties, Mater. Des. 192 (2020) 108694, http://dx.doi.org/10.1016/j.matdes.2020.108694.

[52] F. Huang, X. Xu, X. Lu, M. Zhou, H. Sang, J. Zhu, The exchange bias behavior of $BiFeO_3$ nanoparticles with natural core-shell structure, Sci. Rep.-UK 8 (2018) 2311, http://dx.doi.org/10.1038/s41598-018-19676-5.

[53] S. Vijayanand, M.B. Mahajan, H.S. Potdar, P.A. Joy, Magnetic characteristics of nanocrystalline multiferroic $BiFeO_3$ at low temperatures, Phys. Rev. B 80 (2009) 064423, http://dx.doi.org/10.1103/PhysRevB.80.064423.

[54] N. Shamir, E. Gurewitz, H. Shaked, The magnetic structure of $Bi_2Fe_4O_9$ analysis of neutron diffraction measurements, Acta Crystallogr. A 34 (1978) 662–666, http://dx.doi.org/10.1107/S0567739478001412.

[55] H. Béa, M. Bibes, A. Barthélémy, K. Bouzehouane, E. Jacquet, A. Khodan, J.-P. Contour, S. Fusil, F. Wyczisk, A. Forget, D. Lebeugle, D. Colson, M. Viret, Influence of parasitic phases on the properties of $BiFeO_3$ epitaxial thin films, Appl. Phys. Lett. 87 (2005) 072508, http://dx.doi.org/10.1063/1.2009808.

[56] M. Sakar, S. Balakumar, P. Saravanan, S. Bharathkumar, Particulates Vs. fibers: Dimension featured magnetic and visible light driven photocatalytic properties of Sc modified multiferroic bismuth ferrite nanostructures, Nanoscale 8 (2016) 1147–1160, http://dx.doi.org/10.1039/C5NR06655G.

[57] J.F. Scott, M.K. Singh, R.S. Katiyar, Critical phenomena at the 140 and 200 K magnetic phase transitions in $BiFeO_3$, J. Phys. Condens. Matter 20 (2008) 322203, http://dx.doi.org/10.1088/0953-8984/20/32/322203.

[58] D. Parker, V. Dupuis, F. Ladieu, J.-P. Bouchaud, E. Dubois, R. Perzynski, E. Vincent, Spin-glass behavior in an interacting γ-Fe_2O_3 nanoparticle system, Phys. Rev. B 77 (2008) 104428, http://dx.doi.org/10.1103/PhysRevB.77.104428.

[59] M.K. Singh, W. Prellier, M.P. Singh, R.S. Katiyar, J.F. Scott, Spin-glass transition in single-crystal $BiFeO_3$, Phys. Rev. B 77 (2008) 144403, http://dx.doi.org/10.1103/PhysRevB.77.144403.

[60] T.D. Rao, S. Asthana, Evidence of improved ferroelectric phase stabilization in Nd and Sc co-substituted $BiFeO_3$, J. Appl. Phys. 116 (2014) 164102–164109, http://dx.doi.org/10.1063/1.4898805.

[61] S.M. Selbach, T. Tybell, M.-A. Einarsrud, T. Grande, Size-dependent properties of multiferroic $BiFeO_3$ nanoparticles, Chem. Mater. 19 (2007) 6478–6484, http://dx.doi.org/10.1021/cm071827w.

[62] A.P. Ramirez, Strongly geometrically frustrated magnets, Annu. Rev. Mater. Sci. 24 (1994) 453–480, http://dx.doi.org/10.1146/annurev.ms.24.080194.002321.